630. Combination of time reversal process and ultrasonic tomography approaches for baseline-free damage diagnosis

Yongming Feng[1], Li Zhou[2]
[1,2] College of Aerospace Engineering, Nanjing University of Aeronautics and Astronautics
Yudao street No. 29, Nanjing, Jiangsu, 210016, China
E-mail: [1]*ymfeng@nuaa.edu.cn*
E-mail: [2]*lzhou@nuaa.edu.cn*

(Received 23 March 2011; accepted 15 May 2011)

Abstract. Lamb wave time reversal method is a new and promising baseline-free damage detection technique for structural health monitoring. With this method, damage can be detected without baseline data. In the paper an online damage detection and identification method is presented using time reversal Lamb waves method and ultrasonic tomography for damage diagnosis of composites. The principle and features of the time reversal lamb waves in a composite plate have been introduced firstly. Then the time reversal method has been adapted to detect the local defects in composite plate structures by using active sensing system mounted on a composite plate to excite and receive Lamb waves. This method can identify the location and size of the damage in a composite plate quickly without relying on past baseline date. The image that indicates the damage can be obtained by the ultrasonic tomography algorithm. Experimental results demonstrate the applicability and effectiveness of the proposed method.

Keywords: Lamb waves, time reversal, ultrasonic tomography, damage localization.

1. Introduction

Structural health monitoring (SHM) is an emerging research area with multiple applications in the evaluation of the safety and reliability of critical structures. A typical SHM system for in-situ structural interrogation consists of a network of piezoelectric (PZT) sensors and the unit for data collection and interpretation. PZT sensors in the system are small surface-mounted transceivers capable of generating and detecting Lamb waves in thin-wall structures [1]. As guided waves, Lamb waves can travel for long distance with little amplitude loss and permit the inspection of large areas of thin-wall structures from a single location [2]. Some examples of SHM with Lamb waves include crack detection in aluminum plates, delamination detection in composite plates and corrosion detection in pipes [3–5].

Application of Lamb waves for SHM is complicated due to existence of at least two modes at any given frequency and because of dispersion nature of the modes. When a guided wave mode is dispersive, an initial excitation starting in the form of a pulse of energy will spread out in space and easily get overlapped with the reflection from the defects in the structure. This fact diminishes the spatial resolution and makes experimental data hard to interpret, especially for long distance testing. Some researchers have tried to compensate this dispersion numerically by taking into account the dispersion characteristics of the guided wave modes. However, their work needs accurate group velocity data for the structure, involves extensive computation, and is not effective for real-time SHM system [6, 7].

Furthermore, traditional guided wave SHM techniques developed from nondestructive evaluation (NDE), such as pitch-catch method, pulse-echo method, etc., depend on the availability of a pristine structure baseline to assess the structural health. The detection is performed through the examination of the guided wave amplitude, phase, dispersion and the time of the flight in comparison with the "pristine" situation. These methods may be sensitive not only to small changes in the material stiffness and thickness, but also to the temperature changes. The baseline measured at one temperature, may not be a valid baseline for the measurement made at another temperature. Moreover, maintenance of the baselines database needs extensive memory space. All these aspects limit the application of guided waves for SHM.

Recently, attention has been paid to the time reversal method developed in modern acoustics to compensate the dispersion of Lamb waves and to improve the signal-to-noise ratio of propagating waves [8–11]. For instance, a pulse-echo time reversal method, that is, the time reversal method working in pulse-echo mode has been employed to identify the location and size of defects in a plate [9–11]. In the time reversal method, an input signal can be reconstructed at an excitation point (point A) if an output signal recorded at another point (point B) is reemitted to the original source point (point A) after being reversed in a time domain as illustrated in Fig. 1. This time reversibility (TR) of waves is based on the spatial reciprocity and time reversal invariance of linear wave equations [12, 13]. The specific goal of the research described in this paper is to reconstruct the known excitation signal at the original input location through the time reversal process of Lamb waves. In this study, an enhanced time reversal method is proposed so that the reconstruction of the input signal can be achieved for Lamb wave propagation. The ultimate goal is to use this TR of Lamb waves for damage diagnosis.

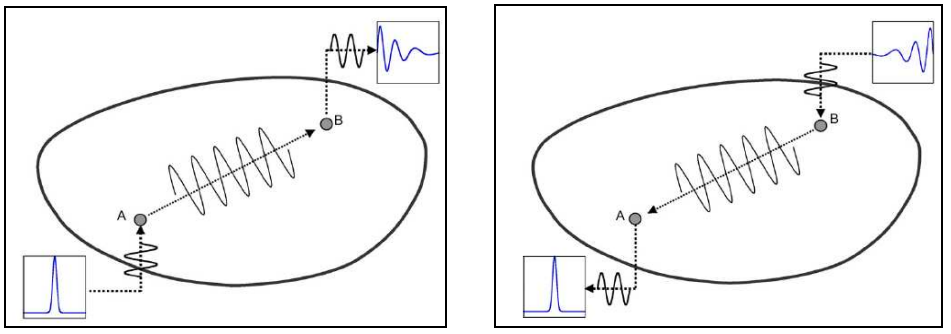

(a) exerting input waves (b) reemitting response waves being reversed with time

Fig. 1. Time reversal concept

Although the application of the time reversal concept to Lamb waves is not a new idea [8,12], the full reconstruction of the input signal has not been attempted before for Lamb waves. To achieve this goal, a specific narrowband input waveform is employed to enhance the TR of Lamb waves. The complete reconstruction of the input signal cannot be achieved when a broadband excitation is employed for Lamb wave propagations. Due to the frequency dependence of the time reversal process of Lamb waves, different frequency components of the broad-band excitation are scaled differently during the time reversal process and the original input signal cannot be fully restored. This is the primary reason for using a narrowband excitation. Once this TR is enforced for Lamb waves, our vision is to detect certain types of defects by examining the deviation of the reconstructed signal from the original input signal without relying on any past baseline data.

This paper takes advantage of this time reversal method to identify defects in composite plates. Damage causes wave distortions due to wave scattering during the time reversal process

and it breaks down the linear reciprocity of wave propagation. Therefore, the time reversibility of waves can allow detecting damage, which causes wave distortions along a direct wave path. It should be noted that the proposed damage detection method leaves out unnecessary dependency on past baseline signals by instantly comparing the known input signal to the reconstructed input signal. By eliminating the need for the baseline signals, the proposed damage detection is immune to potential operational and environmental variations throughout the life span of a structure. This paper is organized as follows: Section 2 deals with the characteristics of Lamb waves and the time reversibility of Lamb waves. In particular, some issues crucial to the time reversibility of Lamb waves are briefly discussed. In Section 3, application of the time reversal Lamb waves method for damage detection in a composite plate is introduced and a damage index is substituted into damage detection. In Section 4, Lamb wave ultrasonic tomography approach is described. In Section 5, the validity of the proposed method has been demonstrated through experimental studies of anisotropic composite plate with damage. Finally, this paper is concluded in Section 6 with a brief summary and discussions.

2. Theory of Lamb wave time reversal

2.1. Lamb waves

Lamb waves, a.k.a. guided plate waves, are a type of ultrasonic waves that remain constrained between two parallel free surfaces, such as the upper and lower surfaces of a plate or shell. Lamb wave theory, which is fully documented in several textbooks [14–16], assumes the 3-D wave equations in the form of

$$\begin{aligned} &\frac{\partial^2 \phi}{\partial x^2}+\frac{\partial^2 \phi}{\partial y^2}+\frac{\omega^2}{c_p^2}\phi=0 \\ &\frac{\partial^2 \psi}{\partial x^2}+\frac{\partial^2 \psi}{\partial y^2}+\frac{\omega^2}{c_s^2}\psi=0 \end{aligned} \tag{1}$$

where ϕ and ψ are potential functions, $c_p^2=(\lambda+2\mu)/\rho$ and $c_S^2=\mu/\rho$ are the pressure (longitudinal) and shear (transverse) wave speeds, λ and μ are the Lame constants, and ρ is the mass density. The potentials are solved by imposing strain-free boundary condition at the upper and lower faces of the plate.

Lamb wave in a plate can be modeled in rectangular [17] or cylindrical coordinates [18]. In the first case, Lamb wave is assumed to be straight crested, while in the second case, Lamb wave is assumed to be circular crested. In both cases, by applying the stress-free boundary conditions at the upper and lower surfaces, Rayleigh–Lamb wave equation can be obtained:

$$\frac{\tan\beta d}{\tan\alpha d}=-\left[\frac{4\xi^2\alpha\beta}{\left(\xi^2-\beta^2\right)^2}\right]^{\pm 1} \tag{2}$$

where, d is the half thickness of the plate, c is the phase velocity, and ξ is the wave number, and $\alpha^2=\omega^2/c_p^2-\xi^2, \beta^2=\omega^2/c_s^2-\xi^2$, $\xi^2=\omega^2/c^2$ The plus sign corresponds to symmetric (S) motion and the minus to anti-symmetric (A) motion. Eq. (2) accepts a number of eigenvalues, $\xi_0^S,\xi_1^S,\xi_2^S,\cdots$ and $\xi_0^A,\xi_1^A,\xi_2^A,\cdots$ respectively. To each eigenvalue corresponds a Lamb wave mode shape. The symmetric modes are designated *S*0, *S*1, *S*2, ... , while the anti-symmetric are designated *A*0, *A*1, *A*2, ...

Since the coefficients α and β in Eq. (2) depend on the angular frequency ω, the eigenvalues ξ_i^S and ξ_i^A are functions of the excitation frequency. The dispersion curve can be expressed in terms of the product of the excitation frequency and the plate thickness versus the group velocity c_g, which is defined as.

$$c_g = d\omega / d\xi \tag{3}$$

For a uniform plate with constant thickness, the dispersion curve can be represented as a function of the frequency as illustrated in Fig. 2. The change of wave speed with frequency produces wave dispersion of a wave packet. At a given frequency thickness product fd, each solution of the Rayleigh–Lamb equation generates a corresponding Lamb wave speed and a corresponding Lamb wave mode. Also, there exists a threshold frequency value determined by the material of the plate and the plate thickness, below which, only *S*0 and *A*0 modes exist. At low frequencies, the *S*0 Lamb wave mode can be approximated by an axial plate wave; and the *A*0 Lamb wave mode can be approximated by a flexural plate wave.

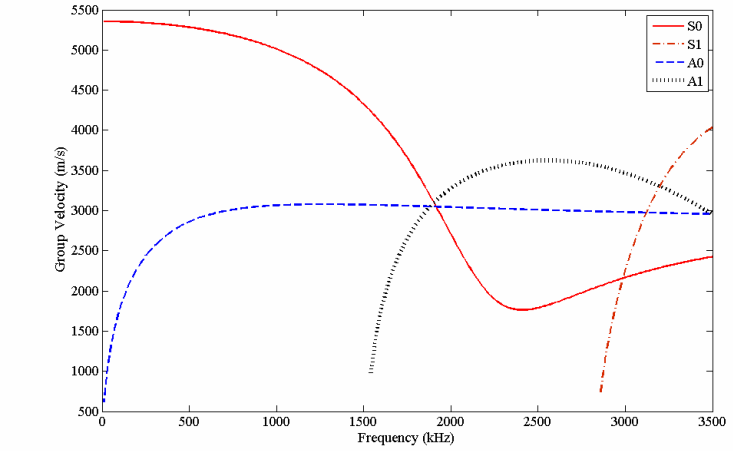

Fig. 2. Group velocity curves of low modes in 1 mm thick aluminum plate

When an arbitrary PZT patch (A) is used as an actuator and another distinct PZT patch (B) is used as a sensor, as shown in Fig. 1, the response voltage at the sensing PZT patch B can be represented as follows:

$$V_B(r,\omega) = K_s(\omega)\hat{E}_B(r,\omega) \tag{4}$$

where r, $V_B(\omega)$, K_s and $\hat{E}_B(\omega)$ are the wave propagation distance from the center of the actuating PZT patch to the sensing PZT patch, the response voltage at the sensing patch B, the mechanical-electro-efficiency constant and the surface strain at the center of patch B with respect to the angular frequency ω, respectively. The surface strain at patch B can be rewritten as follows:

$$\hat{E}_B(\omega) = \hat{I}_A(\omega)K_a(\omega)G(r,\omega) \tag{5}$$

where $\hat{V}$, K_a and G are the input voltage at patch B, the counterpart of the mechanical-electro-efficiency K_s in Eq. (4) and the frequency response function of patch B as a result of the input at patch A, respectively.

Specifically, the frequency response function G is obtained by applying appropriate transformation techniques in the spatial domain and the time domain to the wave equations based on the Mindlin plate theory [14]:

$$G(r,\omega) = -\frac{i\pi h^2}{2D}\frac{\gamma_1 k_1^3 a J_1(k_1 a) H_0^{(1)}(k_1 r)}{k_1^2 - k_2^2} \tag{6}$$

where D, γ_1, a, J_1 and $H_0^{(1)}$ are the flexural stiffness of the plate, the ratio of the dilatational wave to the vertical wave motion of the plate at the wave number k_1, the radius of PZT patch A, the first-order Bessel function and the zero-order Hankel function of the first kind, respectively. The wave numbers, k_1 and k_2 determined at the $A0$ mode and the second flexural $A1$ mode of the plate, respectively. The propagation of the $A0$ mode can be numerically simulated by using Eq. (5). This numerical prediction will be compared with experimental results in a subsequent session. Note that the Bessel function in Eq. (6) is not only a function of the PZT radius (a) but also affected by the wave number (k_1). Because the wave number is a function of the density, flexural stiffness and thickness of the plate, the wave propagation characteristics described in Eq. (6) depend on the fundamental properties of the plate.

2.2. Time reversal Lamb waves

The origin of the time reversal method traces back to time reversal acoustics [9, 11]. In time reversal acoustics, an input body wave can be exactly reconstructed at the source location if a response signal measured at a distinct location is time-reversed (literally the time point at the end of the response signal becomes the starting time point) and reemitted to the original excitation location. This phenomenon is referred to as TR of body waves and has been used in applications such as lithotripsy, ultrasonic brain surgery, non-destructive evaluation and acoustic communications [9].

While the time reversal method for non-dispersive body waves in fluids has been well-established, the study of the time reversal method for Lamb waves on plates is still relatively new. Because of the dispersion characteristic of Lamb waves, wave packets traveling at higher speeds arrive at a sensing point earlier than those traveling at lower speeds. However, during the time reverse process at the sensing location, the wave packets, which travel at slower speeds and arrive at the sensing point later, are reemitted to the original source location first. Therefore, all wave packets traveling at different speeds concurrently converge at the source point during the time reversal process, compensating for the dispersion. The application of the time reversal method to Lamb wave propagation can compensate the dispersion effect, which has limited the use of Lamb waves for damage detection applications [7, 8]. The effect of dispersion on the time reversal analysis of Lamb waves in a homogeneous plate was first studied by Wang et al. [19] by introducing the time reversal operator into the Lamb wave equation based on Mindlin plate theory.

While a number of experimental results have shown that the dispersion of Lamb waves is well compensated through the time reversal process, the TR of Lamb waves has not been fully investigated unlike that of body waves. This study employs a narrowband excitation signal, not only to reduce the frequency dependence of the time reversal process to an acceptable tolerance level, but also to achieve a full reconstruction of the input signal.

With reference to Fig. 3, once a response signal, due to the original input signal at PZT patch A, is measured at PZT patch B, the reconstructed input signal at PZT patch A can be obtained by reemitting the time-reversed response signal at PZT patch B. Note that the time reversal operation of a signal in the time domain is equivalent to taking the complex conjugate of the Fourier Transform of the signal in the frequency domain. Therefore, the time reverse

operation on the response signal at PZT patch B is equivalent to taking the complex conjugate of Eq. (4) in the frequency domain:

$$\hat{V}_B(r,\omega) = K_S^*(\omega)\hat{E}_B^*(r,\omega) \tag{7}$$

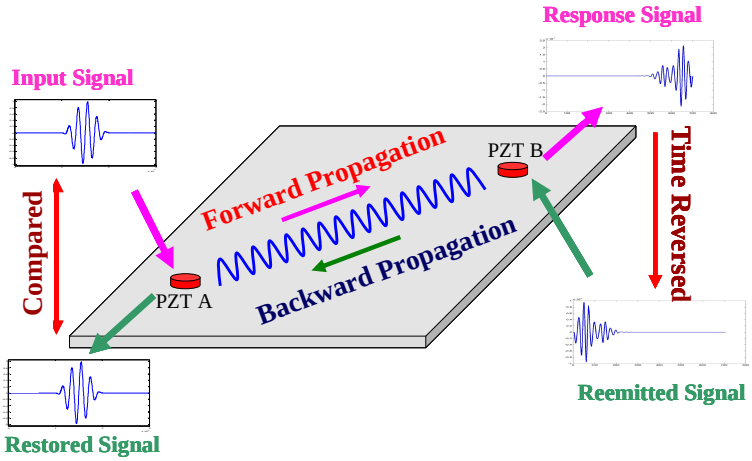

Fig. 3. Generation and sensing of Lamb waves on a plate by using PZT patches

The reconstructed signal at PZT patch A from the reemitted signal at PZT patch B can be represented in a similar fashion as Eq. (4)

$$\hat{V}_A(r,\omega) = K_S(\omega)\hat{E}_A(r,\omega) \tag{8}$$

where

$$\hat{E}_A(r,\omega) = \hat{V}_B^*(r,\omega)K_a(\omega)G(r,\omega) \tag{9}$$

By using Eqs. (5), (7), (8) and (9), the Fourier transform of the reconstructed signal can be rewritten as

$$\hat{V}_A^*(r,\omega) = \hat{I}_A^*(\omega)K_a^*(\omega)K_s^*(\omega)K_a(\omega)K_s(\omega)G(r,\omega)G^*(r,\omega) \tag{10}$$

Performing an inverse Fourier transform, the reconstructed input signal $\tilde{V}_A$ at PZT patch A is

$$\tilde{V}_A(t) = \frac{1}{2\pi}\int_{-\infty}^{\infty}\hat{I}_A^*(\omega)K_{as}^*(\omega)K_{as}(\omega)G^*(r,\omega)e^{i\omega(T-t)}d\omega \tag{11}$$

where K_{as} denotes the product between K_a and K_s and T represents the total time period for the signal. If the TR of waves was satisfied, the reconstructed signal $\tilde{V}_A(t)$ in Eq. (11) would be identical to the time-reversed original signal $I_A(T\text{-}t)$. To directly compare with the original input signal $I_A(t)$ at PZT patch A, Eq. (11) should be time reversed, thus:

$$\tilde{V}_A(T-t) = \frac{1}{2\pi}\int_{-\infty}^{\infty} \hat{I}_A(\omega) K_{TR}(\omega) G_{TR}(r,\omega) e^{i\omega t} d\omega \tag{12}$$

where

$$K_{TR}(\omega) = K_{as}(\omega) K_{as}^{*}(\omega), \qquad G_{TR} = G(r,\omega) G^{*}(r,\omega) \tag{13}$$

Here, K_{TR} is a constant determined by the electro-mechanical efficiency of the PZT patch, and G_{TR} is referred to as a time reversal operator of Lamb waves in the Mindlin plate theory. In Eq. (12), the TR is achieved only if K_{TR} and G_{TR} are independent of the angular frequency ω. However, because the impulse response function $G(r,\omega)$ of a plate structure is frequency dependent and the time reversal operator is defined as $G(r,\omega)G^{*}(r,\omega)$, the time reversal operator G_{TR} varies with respect to the frequency. This indicates that the wave components at different frequency values are non-uniformly scaled due to the fundamental properties of the plate. Therefore, the original input signal cannot be properly reconstructed if a broad-band input signal is used.

To alleviate this problem, a narrowband excitation signal is used with a multi-resolution signal analysis technique so that the time reversal method yields a reconstructed signal sufficiently close to the emitted signal. Note that when a single frequency input is used, the frequency dependence shown in Eq. (13) disappears, allowing for proper reconstruction of the original input signal.

3. Application of time reversal Lamb waves to damage detection in a composite plate

Intact composites possess atomic linear elasticity as water and copper do. The atomic elastic material is well described by the classical linear elastic constitutive law and linear wave propagation equations. However, it should be noted that the atomic elastic materials demonstrate nonlinear mesoscopic elasticity that appears to be much like that in rock or concrete if they have been damaged. Nonlinear mesoscopic elastic materials have hysteretic nonlinear behaviors yielding acoustic and ultrasonic wave distortion, which gives rise to changes in the resonance frequencies as the amplitude of the excitation changes, generation of accompanying harmonics, nonlinear attenuation and multiplication of waves at different frequencies [20, 21]. It has also been shown that cracks and delamination with low-aspect-ratio geometry are the scattering sources creating nonlinear waves, which arise from hysteresis in the wave pressure–deformation relation [22]. Wave scattering can be also caused by either horizontal or vertical mode conversion in which the energy of the incident Lamb waves at a specified driving frequency is redistributed into neighboring Lamb wave modes as illustrated in Fig. 2. Because damage change the internal geometric boundary conditions in a composite plate, diffraction and reflection of the waves can also produce wave scattering when the incident Lamb waves pass through damage.

Because the TR of waves is fundamentally based on the linear reciprocity of the system [12, 13], the linear reciprocity and the TR break down if there exists any source of nonlinearity along the wave path. Therefore, by comparing the discrepancy between the original input signal and the reconstructed signal, damage such as crack opening-and-closing, delamination and fiber breakage could be detected.

In most conventional damage detection techniques, damage is inferred by comparing newly obtained data sets with baseline data from measurements when the condition of the system was good. Because there might have been numerous variations since the baseline data were collected, it would be difficult to blame structural damage for all changes in the measured signals. For instance, operational and environmental conditions may affect the system behavior

and these conditions may be different from those present when the baseline data were collected. Therefore, data normalization, which attempts to distinguish signal changes originated from structural damage from those caused by natural variations of the system, needs to be addressed [18].

In this study, the dependency on the baseline data measured at some previous point in time is completely eliminated by almost instantly comparing the emitted input signal and the reconstructed input signal. Furthermore, the active PZT sensing system employed in this study allows for an easy implementation of the time reversal process. The generation of the input signal, excitation of the actuation PZT and acquisition of the response signal are fully automated and the entire time reversal process for one particular path takes less than a minute.

Our ultimate goal is to estimate damage by comparing the shape of the original input signal with that of the reconstructed signal. The initial input waveform is well restored through the time reversal method when there is no defect in the composite plate tested. A damage index (DI) based on this observation is defined as follows:

$$DI = 1 - \sqrt{\frac{\left\{\int_{t_0}^{t_1} I(t)V(t)\,dt\right\}^2}{\int_{t_0}^{t_1} I(t)^2\,dt \int_{t_0}^{t_1} V(t)^2\,dt}} \tag{14}$$

where the I(t) and V(t) denote the known input and reconstructed signals. t_0 and t_1 represent the starting and ending time points of the baseline signal of the Lamb wave. The value of DI becomes zero when the TR of Lamb waves is preserved. Note that the root square term in Eq. (14) becomes 1.0 if and only if $V(t) = \alpha I(t)$ for all t where $t_0 \le t \le t_1$ and α is a non-zero constant. Therefore, simple linear attenuation of a signal will not alter the damage index value. If the reconstructed signal deviates from the input signal, the damage index value increases and approaches 1.0, indicating the existence of damage along the direct wave path.

One potential advantage of the time reversal analysis is that damage might be inspected without requiring any baseline data to be obtained at some previous time. This advantage over conventional damage detection techniques helps minimize false warnings of damage. For instance, if the operational temperature or boundary conditions of a system change after the baseline data are collected, most pattern recognition techniques will have difficulties in discerning signal changes caused by damage from those due to the temperature or boundary condition changes. In other words, if there are any changes in the newly measured signal since the baseline signal is obtained, it is hard to determine what the cause of this change is. However, by instantly comparing the input waveform with the reconstructed signal, the time-dependent issue of the conventional pattern recognition techniques can be eliminated, making it much easier to distinguish signal changes caused by damage from those caused by natural variation of the system.

4. Lamb wave ultrasonic tomography approaches

Defect detection, growth monitoring and location mapping with guided wave arrays has been studied through computer tomography approaches, using wave speed, attenuation or energy as features for image reconstruction [23, 24]. While accurate defect images can be obtained, however, those approaches are quite time consuming and the sensitivity is not satisfactory with sparse sensors. A simple yet effective correlation analysis technique was developed in this study to detect defects by measuring the differences in the guided wave signals between original and restored using time reversal method.

In order to determine the location of the defect, we assume that the probability of a defect occurrence at a certain point can be estimated from the severity of the signal changes between

original and restored of different sensor pairs as a result of this defect and its relative position to the sensor pairs. The physical intuition behind this is that a defect would cause the most significant signal change in the direct wave path, and that the signal change effect would decrease if the defect is away from the direct path of the sensor pair. (Note that there might be cases that mirror reflection exists with the defect and the above assumption does not apply; the statistical nature of multiple sensor pairs can accommodate it to some extent.)

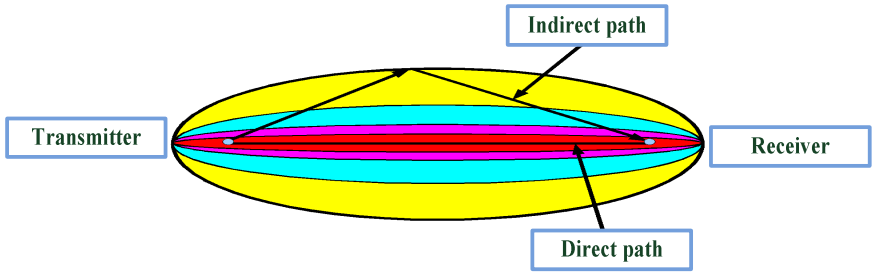

Fig. 4. Illustrations of the elliptical distribution function of the RAPID algorithm

Defect distribution probability within the sensor network can thus be expressed as a linear summation of all the signal change effects of every possible transmitter-receiver pair, each of which has a spatial distribution. Here a simple linearly decreasing elliptical distribution is assumed shown in Fig.4, with the transmitter and receiver PZT at the foci. Assuming there are total N PZT elements in an array cluster of a sensor network, the estimation of the defect probability at position (x, y) within the reconstruction region P(x, y) can be written as:

$$P(x,y) = \left| \sum_{i=1}^{N-1} \sum_{j=i+1}^{N} P_{ij}(x,y) \right|^{\alpha} = \left| \sum_{i=1}^{N-1} \sum_{j=i+1}^{N} DI_{ij} \left[\frac{\beta - RD_{ij}(x,y)}{\beta - 1} \right] \right|^{\alpha} \tag{15}$$

Here, P_{ij} (x, y) is the defect distribution probability estimation from the transmitter i and receiver j sensor pair, D_{ij} is the signal difference coefficient of the sensor pair S_{ij} and following equation (14). α is the signal enhancement factor. Note that, due to reciprocity, the signal collected from sensor pair S_{ji} should be the same as that from S_{ij} , thus only $N(N-1)/2$ sets of data are needed. In the real experiment, the signal of sensor pair S_{ji} was still collected for verification and averaging purpose. $(\beta - RD_{ij}(x, y))/(\beta - 1)$ is the non-negative linearly decreasing spatial distribution function of S_{ij} , with its contour in the shape of a set of ellipses. Figure 4 shows the geometric interpretation of this distribution function. In the formula,

$$RD(x,y) = \begin{cases} \beta, RD(x,y) \geq \beta \\ RD(x,y), RD(x,y) < \beta \end{cases} \tag{16}$$

where:

$$RD(x,y,x_{1k},y_{1k},x_{2k},y_{2k}) = \frac{\sqrt{(x-x_{1k})^2+(y-y_{1k})^2}+\sqrt{(x-x_{2k})^2+(y-y_{2k})^2}}{\sqrt{(x_{1k}-x_{2k})^2+(y_{1k}-y_{2k})^2}} \tag{17}$$

is the ratio of the sum of distance of the point (x, y) to the transmitter i and receiver j (the focal radii) to the distance between the transmitter and receiver. β is a scaling parameter which controls the size of the effective elliptical distribution area, and $\beta > 1$. When $RD_{ij}(x,y) = 1$, i.e. the point (x, y) is on the direct line of the transmitter–receiver pair S_{ij} , $P_{ij}(x, y)=DI_{ij}(x, y)$; when $RD_{ij}(x, y)=\beta$, i.e. the point (x, y) is on the boundary of the effective distribution area, $P_{ij}(x, y)=0$. Usually, β is selected to be around 1.05. Artifacts will be introduced if β is too small, and resolution is lost if β is too large. Generally, if a defect occurs, a set of sensor pair signals will be affected. As a result, in the defect distribution probability image, the point where the defect is located will have dominantly larger probability compared to the other points. Consequently, by applying image processing techniques, such as judiciously selecting a threshold to the defect estimation image, the defect location can be estimated.

5. Experimental study

A composite plate of this study is shown in Fig. 5. The test setup consists of the composite plate with a surface-mounted sensor layer, a personal computer with a built-in data acquisition system and an external signal amplifier. The dimension of the composite plates is 250×250×2 mm. The main instruments used in this experiment are NI PXI-5411 Waveform Generator, K-H Model 7602 Power Amplifier, Tektronix TDS3012 Digital Oscilloscope and computer. The transmitting sensor is activated by applying a narrowband voltage signal given by Eq. (4.1) from a signal generator after amplified by the power amplifier. Then the received signals are displayed by the oscilloscope and analyzed by the computer:

$$V(t) = A[\mathrm{H}(t) - \mathrm{H}(t - n/f_c)](1 - \cos(2\pi f_c t/n))\sin 2\pi f_c t \tag{18}$$

where A is the amplitude modulation of the signal, f_c is the center frequency of the wave, n is the number of the signal cycles and $H(t)$ is Heaviside step function. Figure 6 shows a typical waveform of the signal with the center frequency of 100 kHz.

A commercially available thin film with embedded PZT sensors is mounted on one surface of the composite plate as shown in Fig. 5. A total of 12 PZT patches are used as both sensors and actuators to form an ‘‘active’’ local sensing system. Because the PZTs produce an electrical charge when deformed, the PZT patches can be used as dynamic strain gauges. Conversely, the same PZT patches can also be used as actuators, because elastic waves are produced when an electrical field is applied to the patches. These PZT sensors/actuators are inexpensive, generally require low power and are relatively non-intrusive.

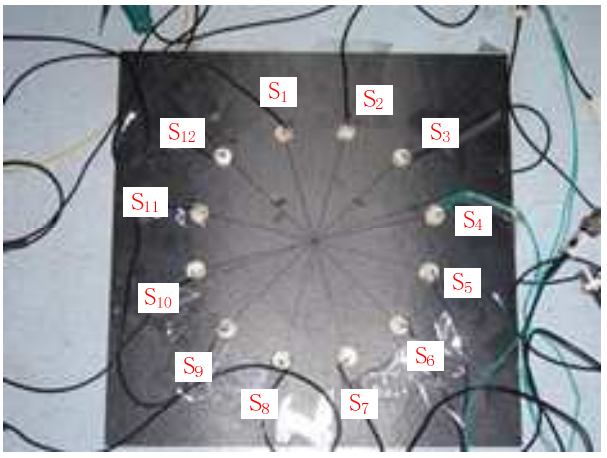

Fig. 5. Composite plate and PZT sensors

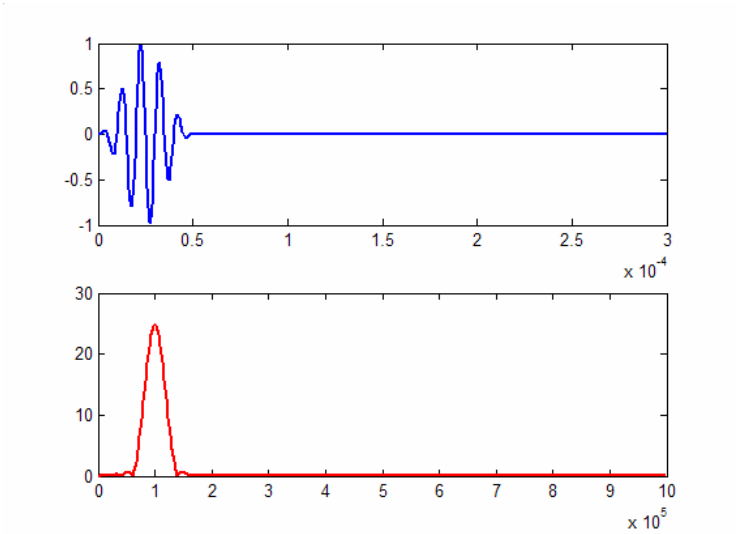

Fig. 6. The excitation signal at the center frequency of 100 kHz

The personal computer has built-in analog-to-digital and digital-to-analog converters, controlling the input signals to the PZTs and recording the measured response signals. Increasing the amplitude of the input signal yields a clearer signal, enhancing the signal-to-noise ratio. On the other hand, the input voltage should be minimized for field applications, requiring as low power as possible. In this experiment, the optimal input voltage was designed to be near 45 V, producing 1–5 V output voltage at the sensing PZTs. For the time reversal analysis, a tone burst excitation is created at 100 kHz so that only two fundamental modes are generated and the magnitude of the time reversal operator is maximized. PZTs in a circular shape are used with a diameter of only 1 cm.

Typical results of the time reversal method obtained from the composite plate used in this study are presented in Fig. 7. First, one PZT patch S6 is designated as an actuator, exerting a predefined waveform into the structure (Fig. 6). Another PZT patch S1 becomes a strain sensor and measures a response signal (Fig. 7(a)). Then the response signal was reversed in time. This processed response signal is reemitted from the previous sensing PZT S1, which is now an actuator. The reconstructed response signal at the original input PZT location is shown in Fig 7(b). This process of the Lamb wave propagation and the time reversal analysis are repeated for different combinations of actuator–sensor pairs. A total of 66 different path combinations are investigated. Finally, the original input signal and the reconstructed signal at the original input point are shown for the actuation PZT S6 and the sensing PZT S1 in Fig. 7(c).

Our ultimate goal is to estimate damage by comparing the shape of the original input signal with that of the reconstructed signal. Results in Fig.7(c) demonstrate that the initial input waveform is well restored through the time reversal method when there is no defect in the composite plate tested. Deal with the damage index the DI of the path of PZT S1 to S6 is 0.06723. Because of measurement error and the inherent properties of composite materials, reversal focusing signal and excitation signal can not be exactly the same. In this study, for the case when there is no damage on the path, the damage index is always smaller than 0.26.

Fig. 8 shows the damage path PZT S3-S9. The measured strain response of the path from PZT S3 to PZT S9 is shown in Fig. 8 (a). The response signal was reversed in time. Then this processed response signal is reemitted from the previous sensing PZT S9.The compared signal of the original input signal (dotted) and the restored signal (solid) is shown in Fig. 8 (c). As can be seen from the figure, the damage path has no obvious focus signal. The damage index of path S3-S9 is 0.963. Table 1 shows the maximum damage index of 12 paths.

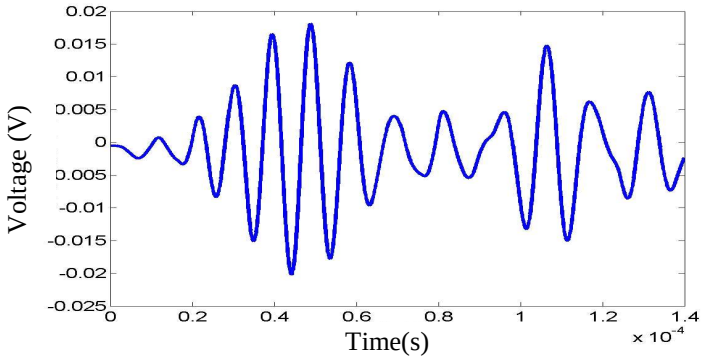

(a)

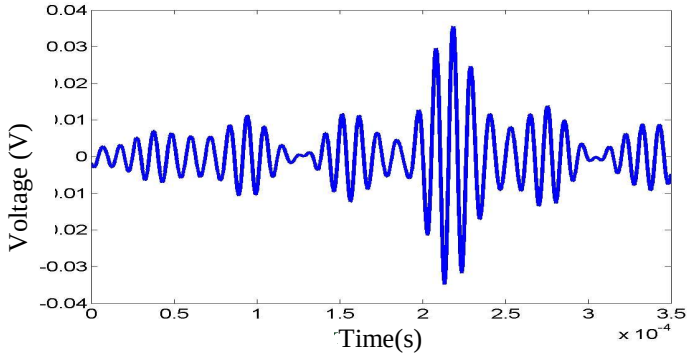

(b)

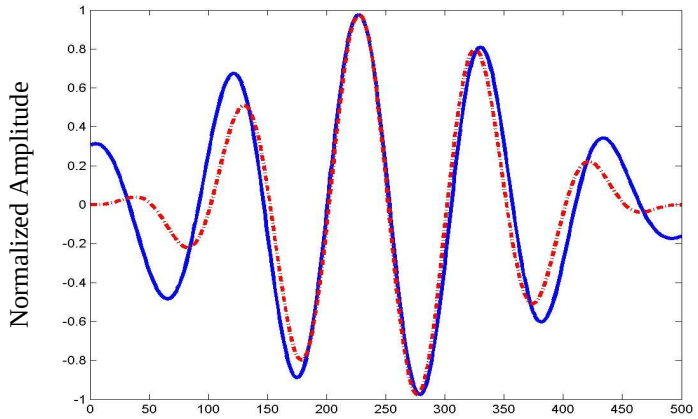

(c)

Fig. 7. The signal of no damage path S1-S6 (a) the measured strain response of the path from PZT S6 to S1.(b) a response signal at the original actuating PZT. S6 (c) the original input signal (dotted) and the restored signal (solid)

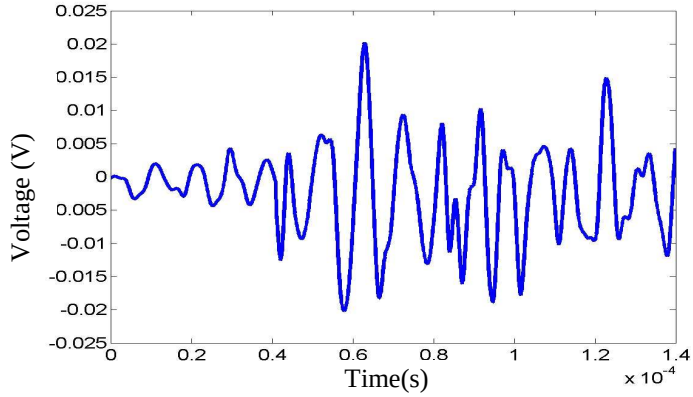

(a)

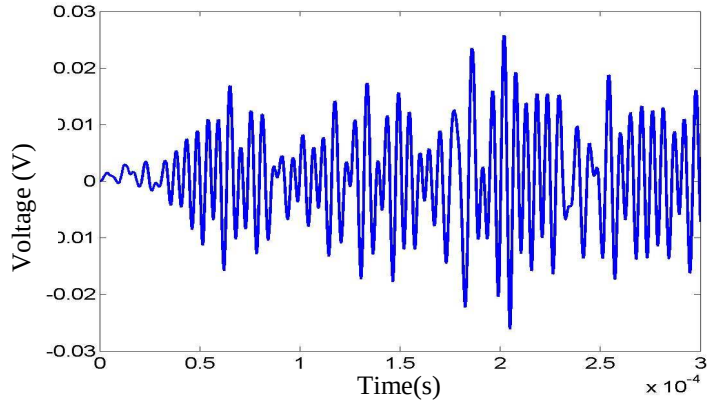

(b)

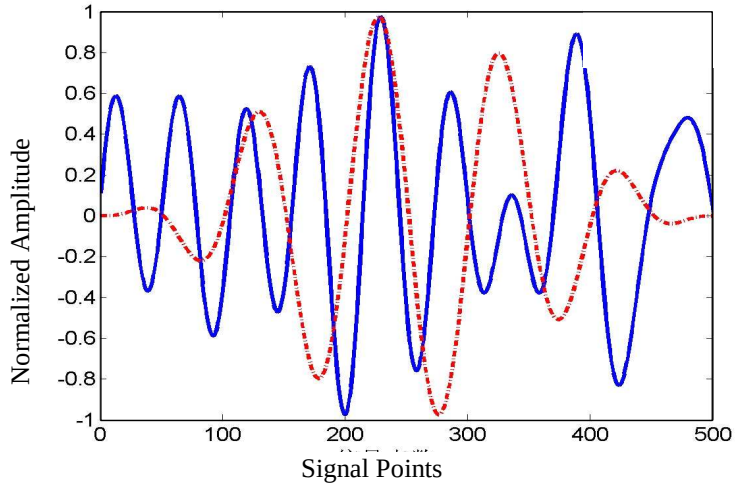

(c)

Fig. 8. The signal of damage path S3-S9 (a) the measured strain response of the path from PZT S3 to PZT S9. (b) a response signal at the original actuating PZT. S3 (c) the original input signal (dotted) and the restored signal (solid)

Table 1. The maximum damage index of 12 paths

Path	DI	Path	DI	Path	DI
1-8	0.945	3-9	0.963	6-10	0.914
1-9	0.561	4-9	0.763	6-11	0.833
2-8	0.680	5-9	0.654	7-10	0.845
2-9	0.885	5-10	0.823	7-11	0.943

Substitution of DI into the RAPID algorithm will result in the damage image. Figure 9 (a) and (b) indicate the damage image when the image factor $\alpha = 1$ and $\alpha = 5$. Figure 9 (c) shows the actual damage using ultrasonic C scan. It can be seen by comparing the obtained by RAPID algorithm and the actual damage image, whether damage location or size are relatively close.

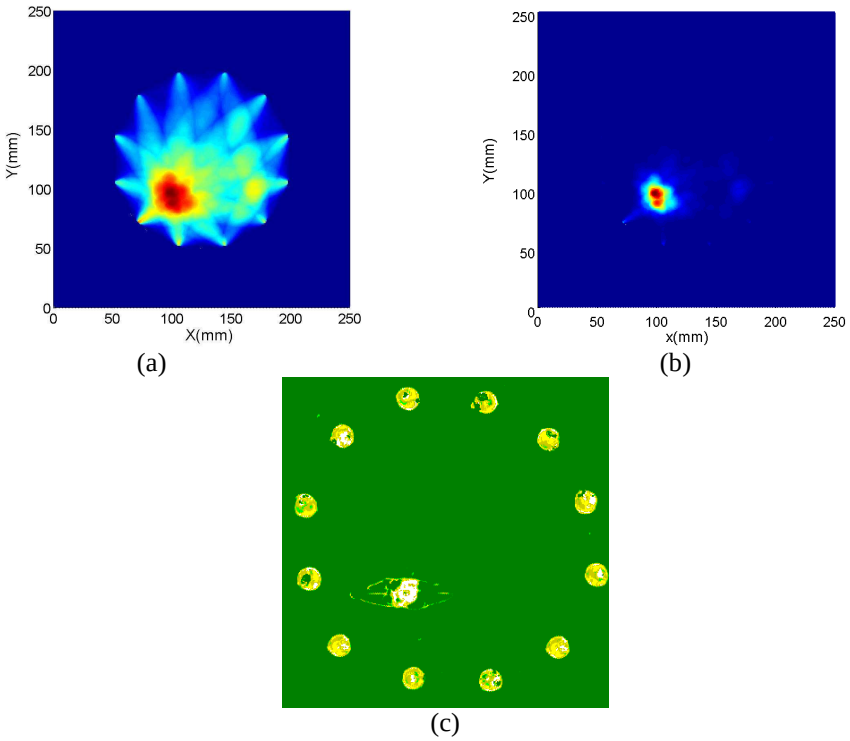

Fig. 9. (a) the damage image when the image factor $\alpha = 1$, (b) the damage image when the image factor $\alpha = 5$, (c) the actual damage image using ultrasonic C scan

6. Conclusions

In this study, the applicability of a time reversal method to health monitoring of a composite plate is investigated. In particular, a unique input waveform is employed to improve the TR of Lamb waves. First, a narrowband excitation waveform is employed to address the frequency dependence of the time reversal operator. By using active sensing system mounted on a composite plate, it has been demonstrated that input waveform exerted at an actuating PZT can be reconstructed at the excitation point after processing the response signal measured at a distance from the excitation point and reemitting the processed signal at the sensing location after being reversed in time. The reconstructed signal will deviate from the known input signal if there are certain types of defects along the wave propagation paths. Then the lamb wave

ultrasonic tomography approaches using the damage index from the time reversal method was investigated. Experimental study results demonstrate the applicability and effectiveness of the proposed method.

The development of the technique is currently underway to classify different representative damage types based on the distortion characteristics between the input waveform and the reconstructed signal. Further research is also warranted to optimally design the parameters of the active sensing system, such as the spacing between the PZT patches, the actuating frequency and the power requirement for the PZTs. It should be pointed out that the procedure developed in this study has only been verified on a relatively simple laboratory test specimen. To fully verify the proposed approach, it will be necessary to apply the proposed approach to different types of representative structures.

Acknowledgments

This work is supported by the Award from National Science of China (No. 10572058), the Research Fund for the Doctoral Program of Higher Education (No. 20050287016), the Science Foundation of Aeronautics of China (No. 2008ZA52012) and Jiangsu Graduate Training Innovation Project (CX09B_070Z).

References

[1] **Giurgiutiu V., Zagrai A.** Characterization of piezoelectric wafer active sensors. J. Intell. Mater. Syst. Struct. 11, 2000. P. 959–976.

[2] **Yu L., Giurgiutiu V.** Design, implementation, and comparison of guided wave phased arrays using embedded piezoelectric wafer active sensors for structural health monitoring. In: SPIE's 13th International Symposium on Smart Structures and Materials and 11th International Symposium on NDE for Health Monitoring and Diagnostics, San Diego, CA, USA.

[3] **Chang F. K.** Built-in damage diagnostics for composite structures. In: Proceedings of the 10th International Conference on Composite Structures (ICCM-10), Whistler, BC, Canada, 14–18 August, vol. 5, 1995. P. 283–289.

[4] **Rose J. L.** Recent advances in guided wave NDE. IEEE Ultrasonics Symposium, 1995. P. 761–770.

[5] **Giurgiutiu V., Zagrai A., Bao J.** Damage identification in aging aircraft structures with piezoelectric wafer active sensors. J. Intell. Mater. Syst. Struct. 15(9), 2004. P. 673–687.

[6] **Sicard R., Goyette J., Zellouf D.** A numerical dispersion compensation technique for time recompression of Lamb wave signals. Ultrasonics, 40(1-8), 2002. P. 727–732.

[7] **Wilcox P.** A rapid signal processing technique to remove the effect of dispersion from guided wave signals. Ultrasonics, 31(3), 2003. P. 201–204.

[8] **Prada C., Fink M.** Separation of interfering acoustic scattered signals using the invariants of the time-reversal operator. Application to Lamb waves characterization, Journal of the Acoustical Society of America, 104 (2), 1998. P. 801–807.

[9] **Ing R. K., Fink M.** Time recompression of dispersive Lamb waves using a time reversal mirror—application to flaw detection in thin plates, IEEE Ultrasonics Symposium 1, 1996. P. 659–663.

[10] **Ing R. K., Fink M.** Time-reversed Lamb waves, IEEE Transactions on Ultrasonics, Ferroelectrics, and Frequency Control , 45 (4), 1998. P. 1032–1043.

[11] **Fink M.** Time-reversed acoustics, Scientific American, 281 (5), 1999. P. 91–97.

[12] **Draeger C., Cassereau D., Fink M.** Theory of the time-reversal process in solids, Journal of the Acoustical Society of America, 102 (3), 1997. P. 1289–1295.

[13] **Fink M., Prada C.** Acoustic time-reversal mirrors, Inverse Problems, 17, 2001. P. R1–R38.

[14] **Viktorov I. A.** Rayleigh and Lamb Waves. Plenum, New York, 1967.

[15] **Graff K. F.** Wave Motions in Solids. Dover, New York, 1975.

[16] **Rose J. L.** Ultrasonic Waves in Solid Media. Cambridge University Press, New York, 1999.

[17] **Giurgiutiu V., Lyshevski S.** Micromechatronics Modeling, Analysis, and Design with MATLAB. CRC Press, Boca Raton, 2004.

[18] **Raghavan A., Cesnik C. E. S.** Modeling of piezoelectric-based Lamb-wave generation and sensing for structural health monitoring. In: Liu, S.-C. (ed.), Smart Structures and Materials 2004: Sensors and Smart Structures Technologies for Civil, Mechanical, and Aerospace Systems. Smart Proceedings of SPIE, Vol. 5391, 2004. P. 419–430.

[19] **Wang C. H., Rose J. T., Chang F. K.** A computerized time-reversal method for structural health monitoring. Proceedings of SPIE Conference on Smart Structures and NDE, San Diego, CA, USA, 2003.

[20] **Guyer R. A., Johnson P. A.** Nonlinear mesoscopic elasticity: evidence for a new class of materials, Physics Today, April 1999. P. 30–36.

[21] **Abeele K. V. D., Johnson P. A., Sutin A.** Nonlinear elastic wave spectroscopy (NEWS) techniques to discern material damage, part I: nonlinear wave modulation spectroscopy (NWMS), Research in Nondestructive Evaluation, 12, 2000. P. 17–30.

[22] **Kazakov V. V., Sutin A., Johnson P. A.** Sensitive imaging of an elastic nonlinear wave-scattering source in a solid, Applied Physics Letters, 81 (4), 2002. P. 646–648.

[23] **Malyarenko E. V. and Hinders M. K.** Lamb wave diffraction tomography, Ultrasonics, 39, 2001. P. 269–81.

[24] **Prasad S. M., Balasubramaniam K. and Krishnamurthy C. V.** Structural health monitoring of composite structures using Lamb wave tomography, Smart Mater. Struct., 13, 2004. N. 73–9.